https://doi.org/10.1016/j.ijmecsci.2019.06.041 This is the Pre-Published Version.

Mechanical modeling of an auxetic tubular braided structure: experimental and numerical analyses

Yu Chen, Ning Jiang, Hong Hu*

Institute of Textile and Clothing, The Hong Kong Polytechnic University, Hung Hom, Kowloon, Hong Kong

* Corresponding author: hu.hong@polyu.edu.hk (Hong Hu); Tel.: +852-3400-3089

Abstract An auxetic braided structure was developed in our previous work for overcoming the slippage problem encountered in the double-helix yarn. However, the influences of the micro-geometric parameters on the macroscopic behavior, which are significant for the structure's design and application, have not been addressed yet. By using a standard tubular braiding technology, several samples of the auxetic braided structure were first fabricated in this work and the design concept and manufacture process were described in detail. Then, systematic parameters studies were completed through experimentally validated finite element models. The study showed that the braided structure could achieve a robust auxetic behavior and its Poisson's ratio and stiffness were strongly dependent on their initial micro-geometric parameters, especially initial braiding angle and diameter of component yarns. A maximum negative Poisson's ratio of -9.49 could be achieved by lowering the angle value to 15°. Higher negative Poisson's ratio effect could obtained with grosser stiff yarn and finer elastic yarns. However, the existence of the elastic wraps would diminish the auxeticity of the braided structure, which should be taken into consideration in design and application.

Keywords Negative Poisson's ratio; Tubular braided structure; Mechanical properties; Parameter studies.

1. Introduction

In general, there are two main approaches for material property enhancement. One is changing the chemical compositions, prime example being the composites (e.g. the fiber reinforced composites [1] and the bionanocomposites [2, 3]). The other is tailoring the material distribution or arrangement. Some specific micro- arrangements in materials allow us to achieve unusual and, sometimes, even unprecedented properties, such as auxetic (negative Poisson's ratio, NPR), negative stiffness, negative refraction index and negative thermal expansion.

In contrast to most of conventional materials with positive Poisson's ratio (PPR), auxetic materials display a counterintuitive phenomenon, that is, they laterally expand

rather than contract when stretched. Over the past three decades, auxetic materials have received considerable attentions owing to the NPR-induced superior mechanical or physical performances, such as dome shape on out-of-plane flexure, improved shear stiffness, indentation resistance, fracture toughness and energy absorption capability [4]. Auxetic materials have been reported early and admitted to exist widely in nature, examples being single crystals of arsenic [5] and cadmium [6], α-cristobalite [7], and many cubic elemental metals. In addition, auxetic behavior in some biological tissues, like cat skin [8], cow teat skin [9] and cancellous bone [10] was also found. However, it was until the pioneering work by Lakes [11] that people realized that the auxetic materials could be obtained in a man-made way. Since then, a large amount of auxetic materials or structures have been developed, synthesized or fabricated from the macroscopic to the molecular levels [11-14].

It is well known that the auxetic effect originates from the micro-topologies and the way they deform under loading, which are the foundation that can be utilized to classify auxetic materials. Three well established basic structures for auxetics have been identified: re-entrant, chiral and rotating rigid structures [15]. The auxetic behavior in all of these systems is fully apparent at small deformation while there are some special materials or structures which exhibit auxetic behavior over a wide range of applied strain but show positive Poisson's ratio at small strain. The structures which generate auxetic effect via elastic instability [16-21] are the pretty typical examples in this context. Beyond that, the double-helix yarn (DHY) structure firstly developed by Hook [22] shows the same characteristic. As displayed in Fig.1, the DHY is a multifilament structure consisting of a relatively thicker and lower stiff core filament and a narrower and stiff wrap around it. Both the core and stiff warp are non-auxetic. When the structure is subjected to a tensile load, both the stiff and core filaments are elongated, and thus the structure will contract laterally in the region of small strain. With the strain increasing, the stiff wrap would laterally displace the elastomeric core, causing an overall lateral expansion and thus a NPR.

Work published by previous authors up to now has systematically exploited several key parameters which can affect the behavior of the DHY [24-29], such as starting wrap angle, diameter ratio of wrap to core, yarns' inherent Young's modulus and Poisson's ratio. The DHY was shown to be capable of achieving a very high NPR value and it was also be used to produce desirable composites [30-32] which could be very promising in sports, medical and defense applications. Yet despite all that, some drawbacks when using the DHY exist; one of them is the slippage of the stiff yarn on the surface of the core yarn which would impair its performance. In addition, the uneven surface of DHY would raise trouble during textile production [33]. For offering a solution to these issues, an ingenious design was proposed by Zhang [33] to enclose an external sheath onto the DHY. The sheath can help bind the two components together

as well as act as a protective coating, but it would significantly reduce the maximum NPR value [33, 34]. Also, using a modified circular braiding technique, an improved helical auxetic yarn structure was proposed by the authors [34] via adding an additional braided sheath between the stiff yarn and the core in order to better fix the stiff one. However, a relatively complex manufacturing process is needed for the improved helical auxetic yarn although it can weaken the slippage.

Another new type of auxetic braided structure which can be produced by using standard circular braiding technique was proposed by the authors [35]. Before, the authors had investigated the difference in auxetic behavior between the new braid and DHY by experiments. The previous work has demonstrated that the new design is possible to achieve NPR effect and the stiff yarn in it is well fixed by the other elastic yarns and thus the slippage problem is overcome. However, detailed parameters studies, which are really meaningful for its improved design and application, have not been involved yet. This paper is a significant addition to our previous work. We described the design concept and manufacture process of the braided structure in detail and conducted an in-depth investigation, both experimentally and numerically, on it. Next, the experimentally validated finite element (FE) models were adopted to explore the effects of the inherent modulus and initial micro-geometric parameters on the macroscopic mechanical behavior of the braided structure.

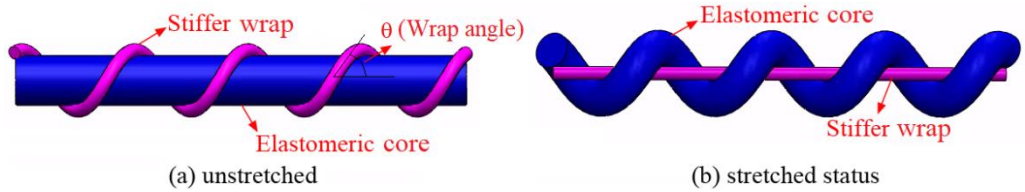

(a) unstretched (b) stretched status

Fig. 1. Double-helix yarn (DHY) structure [22, 23]. (Color online only)

2. Structure and methods

2.1. Geometry of the braided structure

The braided structure firstly proposed in our previous work [35] consists of one core and two sets of helical yarns interlacing in opposite directions, as schematically illustrated in Fig.2. The braided structure includes three components: stiff wrap yarn, low-stiffness elastic wrap yarns and low-stiffness elastic core. Different from the DHY where the stiff yarn is directly wound onto the core, the stiff yarn in this braided structure is now interlaced with other elastic wrap yarns and helically covers the core together with elastic wrap yarns. The same auxetic behavior as the DHY is expected in this braided structure owing to the sharp stiffness gap between the stiff yarn and the core yarn. One prominent characteristic in this interlacement layout is that it would effectively strengthen the interactive constraints between the stiff yarn and the core yarn

so as to overcome the slippage problem in DHY without an additional coated sheath. Structurally, the elastic yarns can effectively help to bind the stiff yarn with the core yarn, but may also limit the lateral displacement of the core yarn to some extent. In this regard, the elastic wrap yarns must not be stiff. Another distinct advantage lies in more flexibility in design compared to the DHY. For instance, desirable performances can be readily achieved by tailoring four key geometrical parameters: initial braiding angle (θ), diameter of the stiff yarn (D_s), diameter of the elastic yarn (D_e) and diameter of the core yarn (D_c). Beyond that, the mechanical parameters, namely the inherent Young's modulus and Poisson's ratio of each component, will also enhance the structure designability. What is more, from the point of view of manufacture, with respect to the sheath-enclosed helical auxetic yarn [33] and the improved helical auxetic yarn [34], the braided structure can be easily produced via a standard tubular braiding process, which may be a great help for its improved design and application.

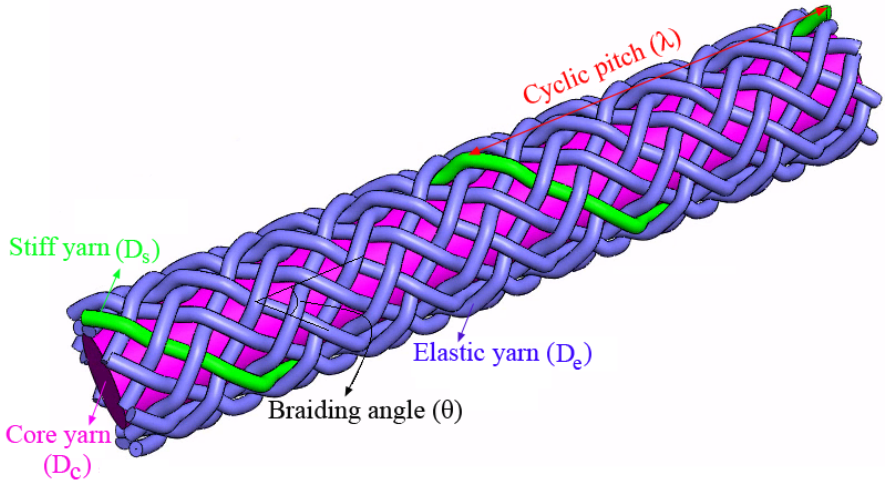

Fig. 2. Geometry of the braided structure firstly proposed in our previous work [35]. (Color online only)

2.2. Methods

2.2.1 Experiment

The criterion for choosing the yarn components was determined according to the design philosophy introduced in section 2.1. The crucial point on the yarns' selection lies in the stiffness rather than the chemical composition. As a result, we used some perfectly ordinary, low cost and store-bought yarns in this paper, instead of synthesizing or fabricating some special ones. The appearance of each yarn component we used is displayed in Fig.3. In the core yarn, a rubber core is covered with a layer of polyester while the stiff and elastic yarns are the common dacron and the spandex, respectively. Basic details for the three yarn components are listed in Tab.1. The nominal (engineering) stress-strain curve for each component, as shown in Fig.4, is the mean

value calculated from three specimens under uniaxial tensile test. The Young's modulus for each component was calculated using the initial linear elastic region of the nominal stress-strain curve while the Poisson's ratio is the mean value we measured from the uniaxial tensile tests.

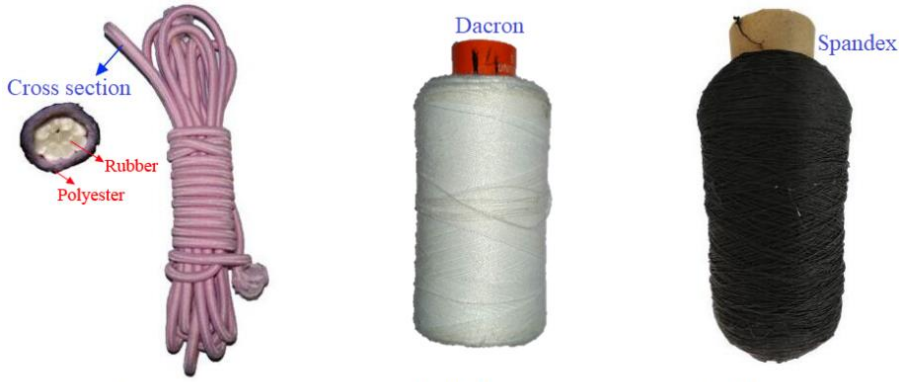

(a) Core yarn (b) Stiff yarn (c) Elastic yarn

Fig.3. Appearances of the yarn components used to produce the braided structure. (Color online only)

Tab.1. Details of the component yarns used.

Component	Yarn constituent	Diameter (mm)	Poisson's ratio	Young's modulus (MPa)
Stiff yarn	Polyester	$D_s = 0.19 \pm 0.01$	0.33	2366
Elastic yarn	Polyester & Rubber	$D_e = 0.32 \pm 0.01$	0.47	19.88
Core yarn	Polyester & Rubber	$D_c = 2.50 \pm 0.14$	0.29	10.14

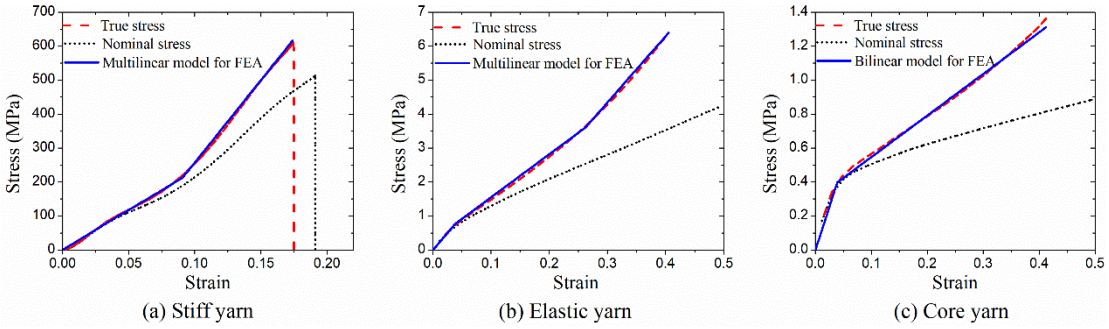

(a) Stiff yarn (b) Elastic yarn (c) Core yarn

Fig.4. Illustration of true and nominal stress-strain curves for each component and the corresponding multilinear or bilinear material model for finite element analysis (FEA): (a) stiff yarn; (b) elastic yarn; (c) core yarn. (Color online only)

As it is easier to manufacture in terms of sample scale, three samples (Fig.5(b)) with a maintained braiding angle (θ=28°) were fabricated for comparison by using the circular braiding machine with 16 yarn carriers (Fig.5(a)). During the preparation process, the core was placed in the center hole of the machine as mandrel and then the stiff yarn was mounted on one selected carrier while elastic yarns filled up the rest

fifteen carries. The carries would be grouped into two equally-sized groups after rotating the machine with one group moving in the clockwise direction and the other group moving in the counterclockwise direction, thus forming a tubular braided structure [35].

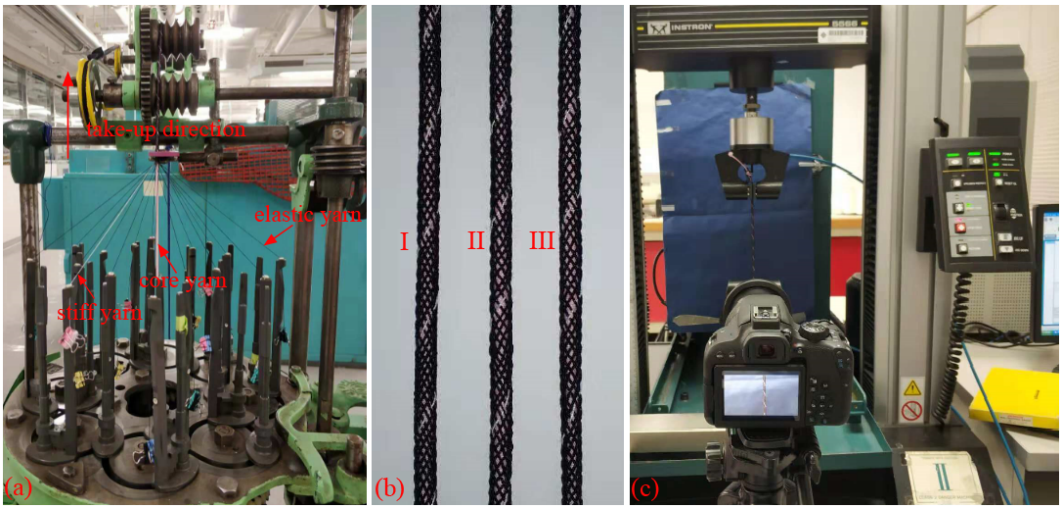

Fig.5. (a) Manufacturing process of the braided structure; (b) photographs of the samples produced; (c) setup of a braid sample on a testing machine. (Color online only)

As displayed in Fig.5(c), tensile tests were performed by using an Instron 5944 tester (Instron Worldwide Headquarters, Norwood, Massachusetts, USA) with a loading cell of 50 N. The sample gauge length for all samples was set as 150 mm. The samples were stretched under a loading speed of 15 $\mathrm{mm \cdot min^{-1}}$ until a failure occurred. While the tensile force (F_L) and the longitudinal strain (ε_L) of each sample were recorded automatically via the Instron testing system, the transversal deformations were captured by using a high-resolution CMOS camera (Canon EOS 800D, Tokyo, Japan). A photograph of the tested specimen was taken at every 1% loading strain during tensile test. In order to better measure the transverse deformation, the captured photographs were further processed by using the software IMAGEJ [32].

Fig.6(a) displays the captured photographs of a sample at several selected loading strains while the corresponding threshold images obtained from IMAGEJ are demonstrated in Fig.6(b). It can be seen that upon stretching, the braid gradually transits from a straight state to a curved shape of quasi-periodic distributed peak-trough. The maximum effective width of the braid along the transverse direction, $\bar{H}$, is the pixel value from peak to trough in the threshold images (see Fig.6(b)), and for accuracy, this value was determined by averaging three adjacent peak-trough distances located in the central position of the braided structure, i.e.,

$$\bar{H} = \frac{1}{3}\sum_{i=1}^{3} H_i \tag{1}$$

Thus, the Poisson's ratio of the braided structure, ν, is given below.

$$\nu = -\frac{\bar{H} - H_0}{H_0 \varepsilon_L} \tag{2}$$

where H_0 denotes the initial transverse width of the structure. In addition, the tensile stress for the braid could be calculated by using the recorded tensile force F_L. For the simplicity of calculation, the cross sectional area of the braid, A, was estimated as,

$$A \approx \frac{\pi\left(D_c + 2D_e + 2\mathrm{Max}\left\{D_e,\ D_s\right\}\right)^2}{4} \tag{3}$$

And then, the tensile stress for all specimens was calculated as,

$$\sigma_L = \frac{F_L}{A} \tag{4}$$

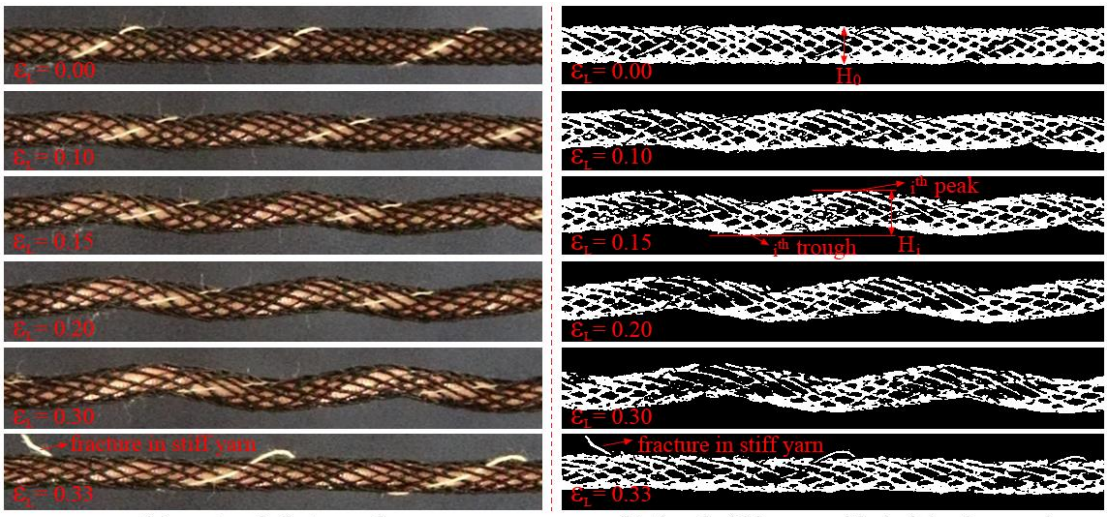

(a) captured photograph (b) threshold image with dark background

Fig.6. Digital Image Processing for structure images obtained. (Color online only)

2.2.2. Finite element analysis (FEA)

The true stress and strain for each component, as displayed in Fig.4, were obtained by using a simple conversion below.

$$\begin{aligned} \varepsilon_t &= \ln\left(1+\varepsilon_n\right) \\ \sigma_t &= \sigma_n\left(1+\varepsilon_n\right) \end{aligned} \tag{5}$$

where σ_t and ε_t are the true stress and strain, and σ_n and ε_n are the nominal stress and strain, respectively. The basic materials for the stiff, elastic and core yarns

were modeled using the simple multilinear or bilinear model (the multilinear model was adopted for the stiff and elastic yarns while the bilinear model for the core yarn) with isotropic hardening, thereby neglecting the possible effect of anisotropy, rate dependency and kinematic hardening. Young' modulus, Poisson's ratio for different components were taken from Tab.1. The density for the stiff, elastic and core yarns was given as $1.39\,g\cdot cm^{-3}$, $1.10\,g\cdot cm^{-3}$ and $1.10\,g\cdot cm^{-3}$, respectively.

Braided structures' computational design in this study was modeled using the SOLIDWORKS 3D CAD software. Firstly, the helical paths of the wrap components around the core were built using a versatile geometrical model proposed by Tuba Alpyildiz [36]. Then, the three-dimensional entity model of the wrap components was developed through the "swept" feature in SOLIDWORKS. Once the model was generated, it would be finally imported into ANSYS/Workbench for analysis and the respective material and its properties would be assigned to each component. It has been shown by McAfee and the co-workers [27] that a successful FE results can be obtained from two-cycle model of DHY and then two-cycle model of the braided structure was thereby chosen in the present work for low computation.

Considering the large deformation of the braided structure and the relatively complex contact among the components, Explicit Dynamics (LS-DYNA Export) module in ANSYS/Workbench was adopted for simulation rather than the Static Structural module. As we know, the implicit iteration in the classical ANSYS or the Static Structural module in Workbench is difficult to guarantee its convergence in the nonlinear deformation situations while the explicit integration in Explicit Dynamics can easily get good results within a reasonable integral time step. The Explicit Dynamics has been proven to be valuable in quasi-static cases [37-40]. However, the problem with the way is that low loading velocity would consume huge computation time while error may increase with the increase of loading velocity. This is an important issue we must seriously consider and the sensitivity of the loading rate will be presented in the following.

To accurately portray the motion between the wraps and core component, a contact type of "Frictional" was set in present FE models. It is well known that the friction coefficient is hard to be determined because it relates to many aspects, including the surface roughness and the contact force. In general, the friction coefficient of fibers ranges from 0.1 to 0.8 and the static friction coefficient, u_s, is slightly larger than the kinetic friction coefficient, u_k. We will also present the sensitivity of friction in the later section.

The "sweep" scheme, which is applicable for the body with regular geometric

configuration, was carried out to mesh the models (see Fig.7(a)) as all yarn components were built with ideal circular section. The meshing size should be adjusted according to the component diameter and to make sure that the yarn surface is smooth enough after being meshed. To this end, the element sizes of 0.055 mm, 0.085 mm and 0.35 mm were selected for 0.19 mm thickness stiff yarn, 0.32 mm thickness elastic yarns and 2.50 mm thickness core yarn, respectively. The boundary conditions are also shown in Fig.7(a). It can be seen that the left surface is fixed in *x*, *y* and *z* directions while the right surface is constrained in *x*, *y* direction but subjected to a displacement of ΔU along the *z* direction. If the node displacements in the *x* and *y* directions were not constrained at both left and right surfaces, the wraps and core would be separated from each other as long as a load is applied. Fig.7(b) displays the deformed braided structure in FE simulation and two pairs of *y*- directional maximum and minimum values in the Y-Z plane were observed. The *y*-directional maximum and minimum values at any moment, which could be easily exported by LS-PrePost (an advanced pre and post-processor that is delivered free with LS-DYNA), were recorded for calculating the lateral width of the deformed braided structure and thereby the Poisson's ratio. We could more expediently and accurately capture the *y*- directional maximum and minimum values by selecting the pick-up points from the X-Y plane, as shown in Fig.7(b).

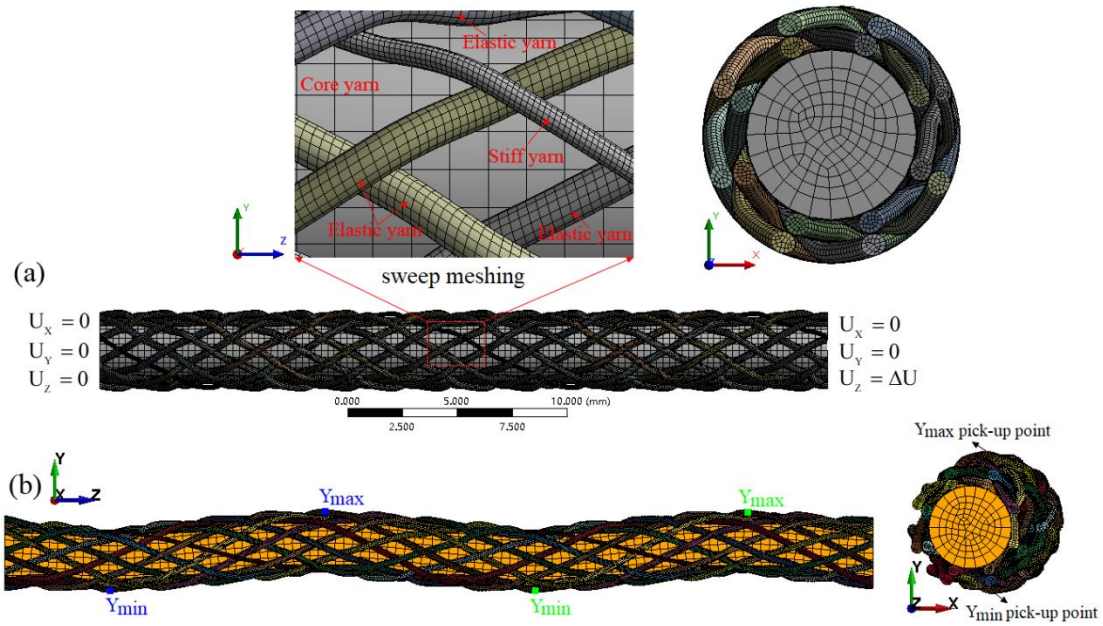

Fig.7. (a) Mesh scheme and boundary conditions in two-cycle model of the new braided structure; (b) measurement of effective diameter from maximum and minimum lateral nodal displacements by using LS-PrePost. (Color online only)

3. Results and discussions

3.1. Validations of FEA

The comparisons of Poisson's ratio and tensile stress between experimental data and FE results with variation values of tensile strain are presented in Fig.8. The initial braiding angle, diameters and intrinsic modulus of each component in the FE models were consistent with those in experimental samples. Poisson's ratio and tensile stress calculated from four levels of loading velocities were compared.

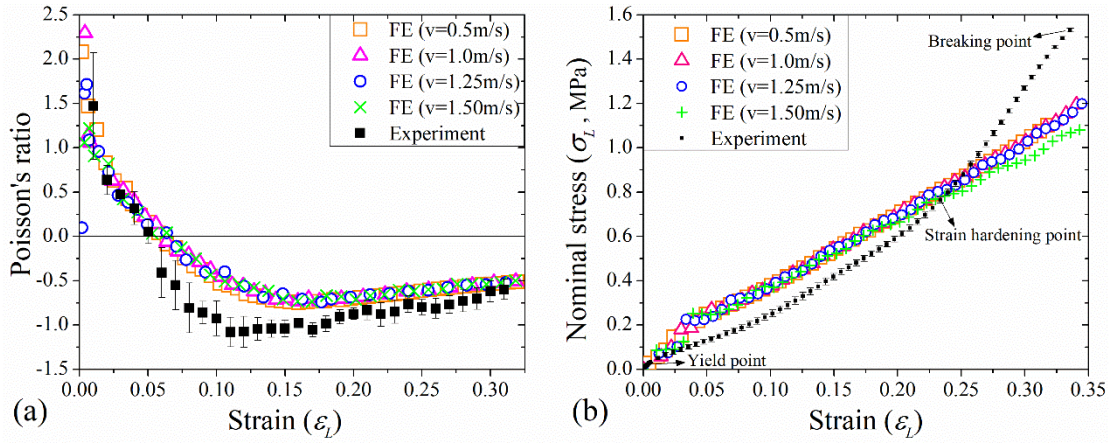

Fig.8. Comparison between FEA and experiment: (a) Poisson's ratio versus strain; (b) nominal tensile stress versus strain. (Color online only)

The loading rate sensitivity analysis has been summarized by Nasim and Etemadi [40] to be one of efficient ways to recognize the quasi-static loading situation and confirm the accuracy. Tab.2 illustrates the needed computation time (estimated by LS-DYNA solver) corresponding to the four levels of loading velocities under the same applied displacement (ΔU) and mesh sizes. It is found that different loading velocities can achieve almost the same Poisson's ratio-strain curves (Fig.8(a)) while the nominal stress-strain curve calculated from the loading velocity of $v=1.50\text{m/s}$ slightly deviates from the curves obtained from the other three lower velocities (Fig.8(b)). It is demonstrated that the loading velocity is converged down to 1.25m/s . More importantly, the needed computation time under 1.25m/s is about two times less than that under 0.5m/s .

Tab.2. Computation time under different loading velocities.

Velocity (m/s)	0.5	1.0	1.25	1.50
Computation Time (hours)	179.97	99.08	78.65	66.45

Considering the strong constraints among the yarns in the braided structure, the friction coefficient in the present FE models was set with a static friction coefficient (μ_s) of 0.8 and a kinetic friction coefficient (μ_k) of 0.75, respectively. Sensitivity analysis of the friction is displayed in Fig.9. It can be seen that the Poisson's ratio and tensile stress are nearly independent of non-zero friction coefficients, which is

consistent with the result obtained by Zeng et al. [41]. Given the above, the following FE analyses are conducted by using the unified setups with $v=1.25\text{m/s}$, $\mu_s=0.8$ and $\mu_k=0.75$.

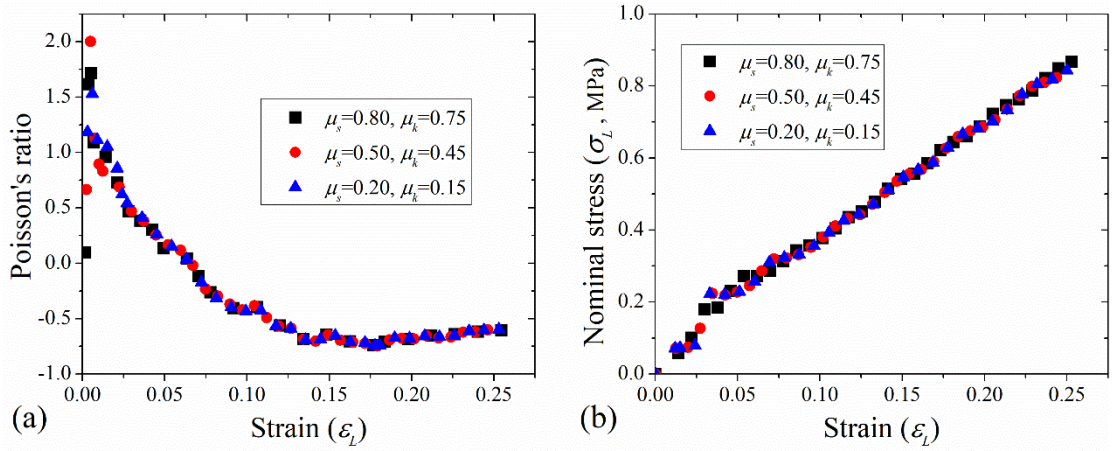

Fig.9. Effect of friction coefficients on: (a) Poisson's ratio; (b) tensile stress ($v=1.25\text{m/s}$). (Color online only)

As shown in Fig.8(a), the FE simulations are close to the experiment data and thus can give a good approximation of the behavior of the braided structure. Actually, a competition exists between the geometrical and material effects of the component yarns in the structure upon stretching. At the start, the applied strain causes the core yarn to contract and the wrap yarns to tighten themselves around the peripheral of the core and hence an obvious decrease in the lateral width of the braided structure. Consequently, a sharp increase to a positive peak in the Poisson's ratio at low strain is observed in the braided structure. With the increase of the applied strain, the extruding between the stiff yarn and the core yarn becomes more and more remarkable. The core yarn will thereby be forced into a helical form, causing an increase in the width of the braid. The material effect gradually loses its dominance and the Poisson contraction of the component yarns is thereby increasingly offset by the geometrical deformation. As a result, the magnitude of the positive Poisson's ratio starts to decrease after the positive peak, and zero even negative value of Poisson's ratio is finally achieved. The point of zero Poisson's ratio, also called critical auxetic point, is observed at around 0.06 strain in Fig.8(a). After the critical point, Poisson's ratio decreases with the strain to a maximum negative value. The mean value of the maximum NPR obtained from experiment is -1.08 while that from FEA is -0.74. With further increasing the strain, the Poisson contraction of the component yarns and the straightening of the stiff yarn will result in a total width shrinking of the braid and thus a reduction in auxeticity can be seen in the FE models after the maximum NPR is reached.

The tensile stress-strain curves obtained from the experiment and FEA, as indicated in Fig.8(b), are highly non-linear. The effective stress was calculated according to Eq.(4). We can find that the curve from the experimental data can be divided into four regimes: linear elastic, yield, strain hardening and fracture. It should be noted that the breaking point in Fig.8(b) refers to the stiff yarn rather than the whole braided structure, as fracture firstly occurs in the stiff one. An approximate linear relation between the tensile stress and strain is observed within the yield stage. Similar approximate linear characteristic can also be found in the curves obtained from FEA. The experimental and numerical effective Young's moduli (mean value), which were calculated by using the initial linear elastic region of the nominal stress-strain curves in Fig.8(b), is 6.46MPa and 5.16MPa, respectively. A general good agreement observed between the experimental and FEA results in Fig.8(b) helps to verify the validity of the FE models we adopted. It can also be found that the effective Young's modulus of the braid is close to that of the core yarn. This is because the tensile stress of the braid is initially dominated by the core yarn, but as the stiff yarn straightens, its influence on the stress of the braid becomes significant. The influence originating from the elastic wraps is relatively small as it is pretty softer compared to the stiff yarn.

The stiff yarn shown in Fig.4 has a greater modulus and ultimate tensile strength than the elastic and core yarns while the elastic and core yarns are able to withstand longitudinal strain more than three times greater than the stiff yarn before failure. Combining different yarns together can take the advantages of each component, thus endowing the new products with special functions. For example, breaking point was observed in the new braid until ε_L=0.335 while an early failure at ε_L=0.191 is found in the stiff yarn (see Fig.8(b) and Fig.4(a)).

Fig.10 displays the relation of the wrap angle θ^* of the stiff yarn with the longitudinal strain. The wrap angle at ε_L=0 is equal to the initial braiding angle (θ) which is $28°$. The angle values at different moments were obtained from the captured photographs during tests. We measured three positions located in the central portion in each sample for accuracy. Average value and error bar of the wrap angle were calculated from the three samples. In the case of FEA, LS-PrePost was used for recording the transient wrap angle of the stiff yarn. Both the experimental and numerical results show that the angle decreases with the increase of the longitudinal strain. We introduced a simple multilinear model to characterize the curves in Fig.10. As it can be seen in the experimental result, there are two inflection points before breaking. A similar trend is observed in the FE result as well. The most notable point is that the decreasing rate in both the experiment and FEA is significantly reduced after θ^* reached the first inflection point and then another fall is observed after crossing the second inflection

point. This indicates that it is becoming more difficult for the stiff yarn to force the core yarn to displace laterally. It would be impossible to fully straighten the stiff yarn as we can find the breaking point occurs at $\theta^* = 6.03°$ rather than $\theta^* = 0°$ according to the experimental result.

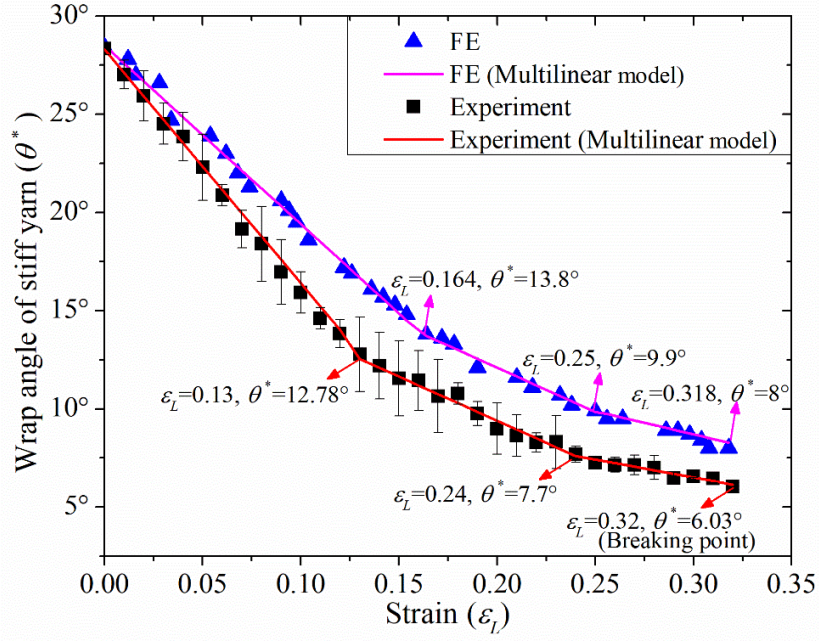

Fig.10. Variation of the wrap angle of stiff yarn with longitudinal strain. (Color online only)

3.2. Parameters studies

Parameters studies can help to seek for the optimal performances of the braided structure, which is significant for its practical applications. The experimentally validated FE model was used for these studies, to further investigate the influences of the yarn component inherent Poisson' ratio and diameter as well as initial braiding angle on the mechanical behavior. Of particular interest to us are the effects from the elastic wraps.

3.2.1. Influence of yarn component diameter

Stiffness ratio of the yarn components, which are closely related with the diameter, is one of the key influences on structure performance. The initial braiding angle for all FE models in this study was kept at $28°$ and the inherent mechanical properties for each component are taken from Tab.1 and Fig.4. We studied two cases here for respectively exploiting the influences from the core/stiff and the core/elastic diameter ratios. The first case was conducted by fixing the diameters of the core and elastic yarns with values of 2.50mm and 0.32mm, respectively, and then tailoring the diameter of the stiff yarn to be 0.19mm, 0.24mm and 0.32mm. Similarly, three diameter levels of 0.19mm, 0.24mm and 0.32mm were endowed to the elastic wraps in the second case while the diameters of the core and stiff yarns were kept as 2.5mm and 0.19mm,

respectively.

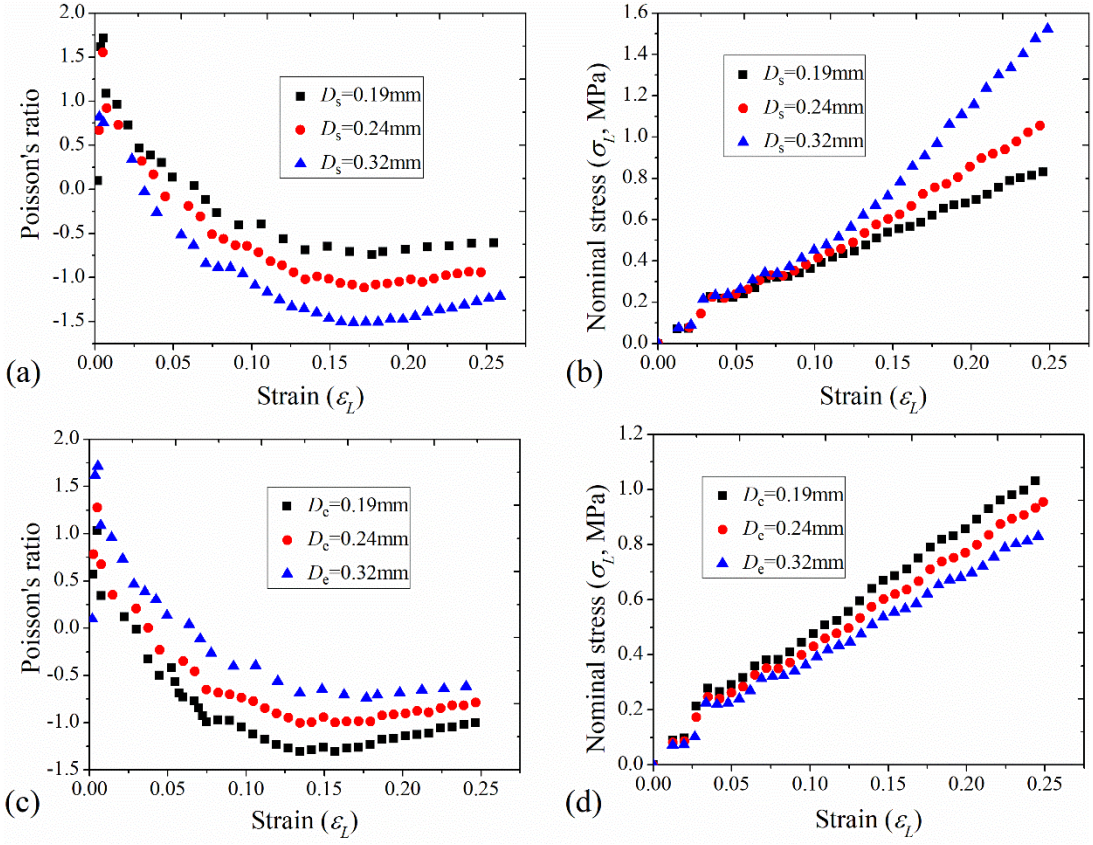

Fig.11. (a) Influence of the stiff yarn diameter, D_s, on the braid's Poisson's ratio and (b) nominal stress; (c) influence of the elastic yarn diameter, D_e, on the braid's Poisson's ratio and (d) nominal stress. (Color online only)

Fig.11 displays the variations of the Poisson's ratio and the nominal tensile stress of the braided structure as a function of strain for different diameters of stiff and elastic yarns, respectively. It is demonstrated in Fig.11(a) that a larger stiff yarn diameter gives a higher maximum NPR value and causes the braid to be auxetic at an earlier rate of strain, as the Poisson's ratio of the braid with a 0.32mm stiff yarn becomes negative at strain of around 0.031 and reaches a maximum negative value of -1.52. The braids with 0.24mm and 0.19mm stiff yarns, by contrast, become auxetic at strain of around 0.042 and 0.065 and achieve a maximum NPR value of -1.12 and -0.75, respectively. Fig.11(b) exhibits that braids have the nearly similar stress values at low strain, but the difference increases with the increase of strain. Apparently, under a large strain, a larger stiff yarn diameter causes a higher nominal tensile stress. This phenomenon can be clarified by a mechanism which has been stated in section 3.1, that is, the tensile stress is dominated by the core at low applied strain and then gradually affected by the stiff yarn with the strain increasing. The stiff yarn with larger diameter makes more contributions to the braid's properties, that is, the braid with thicker stiff yarn will also result in an earlier

strain hardening besides improving the stress.

As displayed in Fig.11(c), the zero-crossing of the Poisson's ratio in the braid with 0.24mm elastic yarn is observed to happen at around $\varepsilon_L = 0.037$ while the braid with 0.19mm elastic yarn becomes auxetic at around $\varepsilon_L = 0.010$; and the maximum NPR values in two cases are -1.02 and -1.32, respectively. Different from the effect of the stiff yarn's diameter, the elastic wrap yarns will prevent the core from displacing laterally and becoming helical, and thus increasing the elastic yarns' diameter causes a later auxeticity and a lower NPR value. Considering an extreme case, the braided structure is degenerated to a DHY when the diameter of the elastic yarns becomes zero. It should be expected that DHY will be more auxetic than the braided structure with the same given stiff and core yarns. Therefore, elastic yarns with large diameter should be voided in the new design for superior auxetic behavior. In addition, the nominal tensile stress is also reduced with D_e increasing, as illustrated in Fig.11(d). There is no doubt that increasing the diameter of the elastic yarns will help to improve their stiffness but may not be going to actually benefit the braid's tensile strength much because of the decisive role of the stiff yarn. According to Eq.(3), the effective stress of the braid is directly dependent upon the cross-sectional area A and therefor the diameter of the elastic yarn. With a little increase in the tensile strength F_L in Eq.(4), increasing the cross-sectional area will result in an dramatic decreases in effective stress, σ_L.

3.2.2. Influence of initial braiding angle

Fig.12 compares the identical models with three different initial braiding angles: $15°$, $28°$ and $40°$. All braids were constructed from the same yarn components with the inherent mechanical properties and diameters as shown in Tab.1 and Fig.4. It can be found from Fig.12(a) to (c) that, the braid with θ=15° becomes auxetic at around ε_L=0.0046 while the critical auxetic point for the braids with θ=28° and θ=40° is ε_L=0.03 and ε_L=0.14, respectively. Also, a maximum NPR value of -9.49 is observed in the $15°$ braid at ε_L=0. 012; the maximum NPR values of -1.52 and -0.43 for $28°$ and $40°$ braids are observed at around ε_L=0.16 and ε_L=0. 38, respectively. This is because the stiff yarn straightens and becomes strained earlier with lower initial braiding angle. The extruding between the stiff yarn and core yarn will thereby arise at low applied strain, resulting in the activation of auxetic behavior

at a lower rate of strain and a higher maximum NPR value.

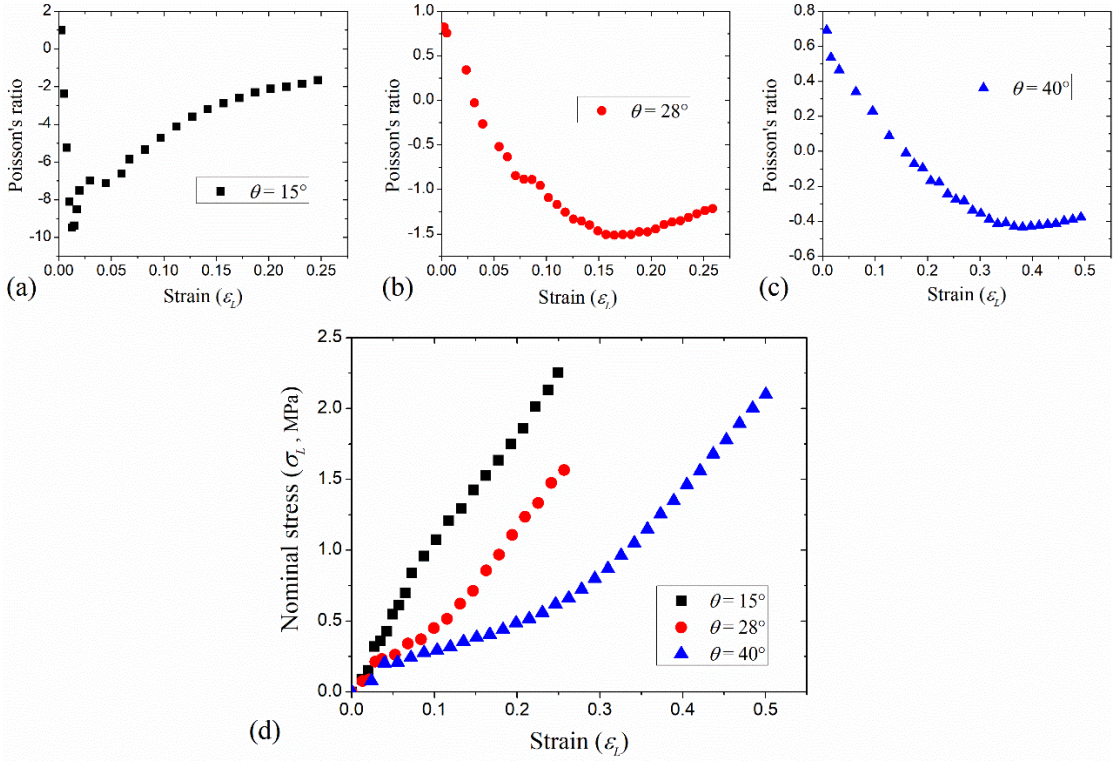

Fig. 12. Influence of the initial braiding angle, θ, on: (a)-(c) Poisson's ratio and (d) nominal stress. (Color online only)

For the nominal stress, it can be found from Fig.12(d) that braid with θ=15° shows slightly higher nominal stress compared to those with θ=28° and θ=40° at low applied strain while a dramatic difference is observed as the strain increases. Increasing the initial braiding angle is seen to result in a lower nominal stress. The reason is that the stiff yarn will not take effect on the braid stress until it becomes tightened and the wrap yarn with larger initial braiding angle tightens itself more slowly than that with lower angle. It is amazing that high stiffness and high NPR value can be achieved simultaneously in the braid which may be impossible in the auxetic honeycombs [42]. Clearly, the initial braiding angle is a quite influential design parameter in altering the auxeticity and stiffness of the braided structure.

3.2.3. Influence of the inherent Poisson's ratio

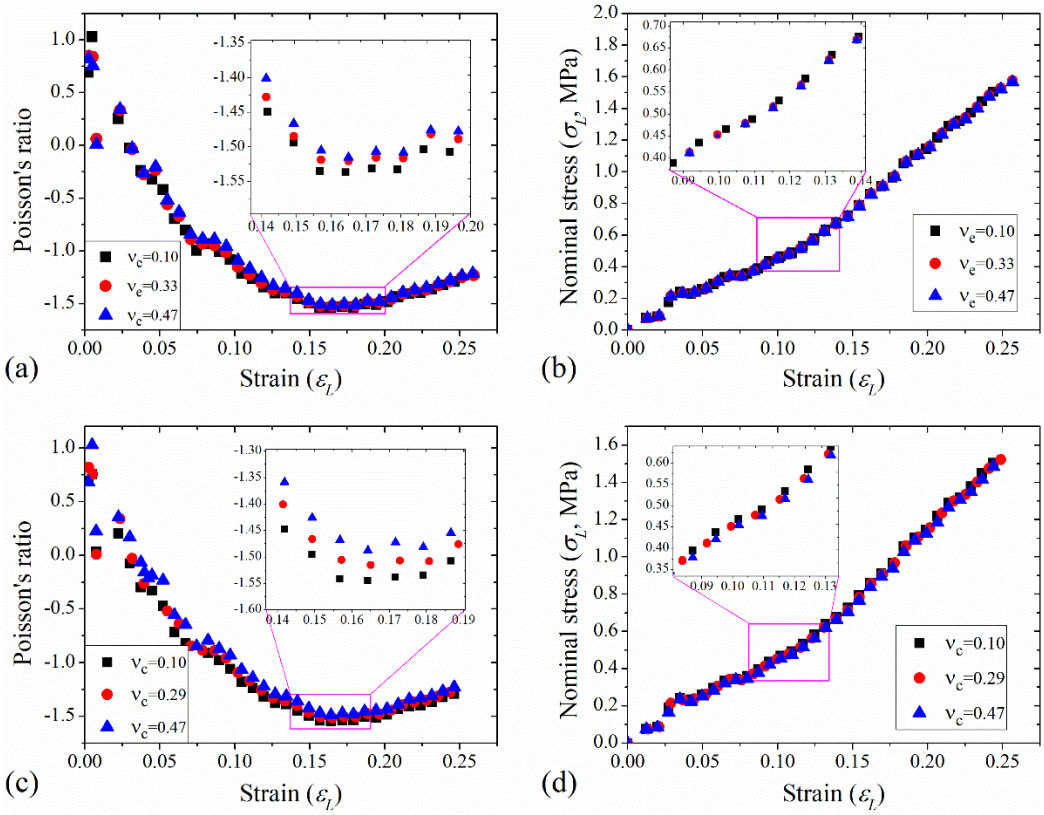

Fig.13. (a) Influence of the inherent Poisson's ratio of elastic yarn, ν_e, on braid's Poisson's ratio and (b) nominal stress; (c) influence of the inherent Poisson's ratio of core yarn, ν_c, on braid's Poisson's ratio and (d) nominal stress. (Color online only)

Fig.13 illustrates the influence of the inherent Poisson's ration of both the elastic and core components on the Poisson's ratio and nominal stress of the braids. All braids used in this topic were endowed with a series of consistent parameters: initial braiding angle ($28°$), inherent Poisson's ratio in stiff component ($\nu_s = 0.33$), elastic yarn diameter (0.32mm), stiff yarn diameter (0.32mm) and core yarn diameter (2.50mm). The results show that increasing ν_e of the elastic components, slightly delays the critical auxetic point and diminishes the maximum NPR value (Fig.13(a)). This phenomenon is due to the fact that larger ν_e leads to a greater Poisson contraction, making the total lateral width of the braid shrink more greatly. Similar mechanism can be used for explaining the deformation behavior depicted in Fig.13(c), that is, earlier auxeticity and higher NPR is achieved in the braid with more compressible core. We can also find that from Fig.13(b) and (d) that the nominal tensile stress of the braid seems to be nearly independent on the Poisson's ratio of both the core and elastic yarns.

3.3. Potential applications

Upon stretching, the stiff wrap in the braided structure tends to straighten, thereby causing the core to displace laterally in a helical manner (see Fig.14(b)). Such special behavior can be adopted to increase the opening of pores in a fabric under tension if two adjacent auxetic braided yarns are out of phase arranged [32] (see Fig.14(c)). Application examples include the blast-proof curtain and smart bandage. In a blast-proof curtain, the size of pores can be manipulated to let explosion shock waves pass through but preventing the flying debris to penetrate. This can reduce the tension applied to the curtain and ensure it doesn't rip under explosion shock [43]. In a smart bandage impregnated with drugs, swelling of wounds would put the bandage under tension, resulting in an automatic release of drugs due to opening up of pores. Compared to the DHY, the braided structure not only mitigates the slippage problem but also shows high flexibility in design. Therefore, the braided structure can be a good alternative for the DHY in the above mentioned applications. In addition, the braided structure also has promising application for clothes that require enhanced shape fit and comfort.

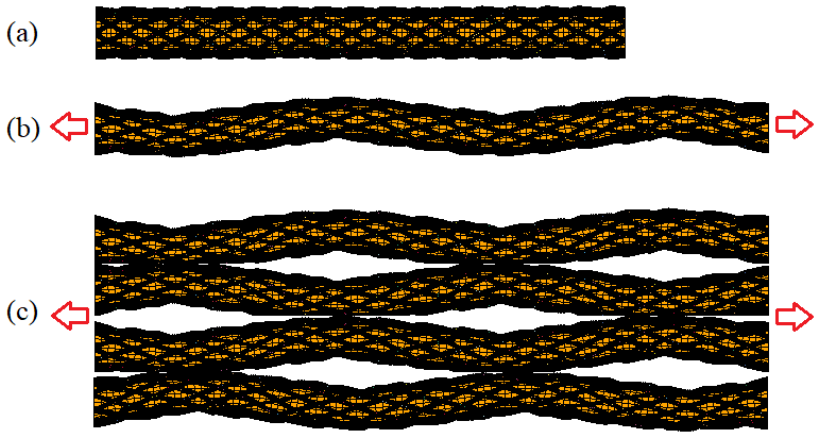

Fig.14. (a) Initial state; (b) auxetic behavior under tension and (c) pores open under tension. (Color online only)

4. Conclusions

A tubular braided structure, which was invented for overcoming the slippage problem in the DHY structure, forms the basis of this paper. Three samples were fabricated on a standard tubular braiding machine and subjected to a uniaxial tensile test. FE models were developed using ANSYS/Workbench and validated with the experiments. Based on the experimentally validated FE modes, influences of parameters were systematically studies. It was found that the initial braiding angle dominates the auxetic behavior of the braid. A maximum NPR of -9.49 could be achieved by lowering the angle value to 15°. In addition, the initial braiding angle also has a big effect on the effective tensile stress of the braid; the lower the angle value, the

higher the stress. Little difference in effective stress could be observed for the braids made with different diameters of stiff and elastic yarns at initial applied strains, but it progressively became obvious with strain increasing. The grosser stiff yarn could result in a higher NPR value and higher effective stress, while for the elastic yarns their influence was opposite. The elastic yarns made a huge contribution to avoid the slippage problem of the stiff wrap yarn and provided more design possibility to achieve a desired Poisson's ratio and stiffness. However, the existence of the elastic wraps would diminish the auxeticity of the braided structure, which should be taken into consideration in design and application.

Acknowledgements

This work was supported by the Research Grants Council of Hong Kong Special Administrative Region Government (grant number 15203615) and The Hong Kong Polytechnic University in form of an internal project (grant number YBUZ).

Conflict of interest statement

The authors declare that they have no conflict of interest.

References

[1] Mallick P K. Fiber-reinforced composites: materials manufacturing and design. New York: Marcel Dekker, 1988.

[2] Ilyas R A, Sapuan S M, Ishak M R, Zainudin E S. Development and characterization of sugar palm nanocrystalline cellulose reinforced sugar palm starch bionanocomposites. Carbohydrate Polymers 2018; 202:186-202.

[3] Jawaid M and Swain SK (eds) Bionanocomposites for packaging applications. Cham, Switzerland: Springer, 2018.

[4] Evans KE, Alderson A. Auxetic materials: Functional materials and structures from lateral thinking! Advanced Materials 2000; 12 (9): 617-628.

[5] Gunton DJ, Saunders GA. The Young's modulus and Poisson's ratio of arsenic, antimony and bismuth. Journal of Materials Science 1972; 7(9):1061-1068.

[6] Li Y. The anisotropy of Poisson's ratio, young's modulus and shear modulus in hexagonal materials. Physica Status Solidi (a) 1976; 38(1):171-175.

[7] Yeganeh HY, Weidner DJ, Parise JB. Elasticity of α-cristobalite: a silicon dioxide with a negative Poisson's ratio. Science 1992; 257(5070):650-652.

[8] Veronda D R, Westmann R A. Mechanical characterization of skin finite deformations. Journal of Biomechanics 1970; 3(1):111-124.

[9] Lees C, Vincent J E, Hillerton J E. Poisson's ratio in skin. Bio-medical Materials and Engineering 1991; 1(1):19–23.
[10] Williams J L, Lewis J L. Properties and an anisotropic model of cancellous bone from the proximal tibial epiphysis. Journal of Biomechanical Engineering 1982; 104(1):50-56.
[11] Lakes R S. Foam structure with a negative Poisson's ratio. Science 1987; 235(4792): 1038-1040.
[12] Yang W. Li Z M , Shi W, Xie B H, Yang MB. Review on auxetic materials. Journal of Materials Science 2004; 39(10):3269-3279.
[13] Wang Z, Hu H. Auxetic materials and their potential applications in textiles. Textile Research Journal 2014; 84(15): 1600-1611.
[14] Alderson A. A triumph of lateral thought. Chemistry & Industry (May) 1999; 384-391.
[15] Zadpoor A A. Mechanical meta-materials. Materials Horizons 2016; 3:371-381.
[16] Ghaedizadeh A, Shen J, Ren X, Xie Y M. Tuning the Performance of Metallic Auxetic Metamaterials by Using Buckling and Plasticity. Materials, 2016, 9(54):1-27.
[17] Mousanezhad D, Babaee S, Ebrahimi H, Ghosh R, Hamouda A S, Bertoldi K, Vaziri A. Hierarchical honeycomb auxetic metamaterials. Scientific Reports, 2015, 5:18306.
[18] Bertoldi K, Reis P M, Willshaw S, Mullin T. Negative Poisson's ratio behavior induced by an elastic instability. Advanced Materials, 2010, 22(3):361-366.
[19] Babaee S, Shim J, Weaver J C, Chen E R, Patel N, Bertoldi K. 3D Soft Metamaterials with Negative Poisson's Ratio. Advanced Materials, 2013, 25(36):5044-5049.
[20] Shen J, Zhou S, Huang X, Xie Y M. Simple cubic three-dimensional auxetic metamaterials. Physica Status Solidi B, 2014, 251(8):1515-1522.
[21] Ren X, Shen J, Ghaedizadeh A, Tian H, Xie Y M. Experiments and parametric studies on 3D metallic auxetic metamaterials with tuneable mechanical properties. Smart Material Structures, 2015, 24(95016):(15pp).
[22] Hook P B, Evans K E, Hannington J P, Hartmann-Thompson C, Bunce T R. Composite materials and structures, U.S. Patent No. US2007031667; 2007.
[23] Aksu A, Tatlıer MS. An investigation on auxetic feature and its applications. International Advanced Researches and Engineering Journal 2018; 02(02):167-176.
[24] Bhattacharya S, Zhang G H, Ghita O, Evans K E. The variation in Poisson's ratio

caused by interactions between core and wrap in helical composite auxetic yarns. Composites Science and Technology 2014; 102: 87-93.
[25] Sloan M R, Wright J R, Evans K E. The helical auxetic yarn e a novel structure for composites and textiles; geometry, manufacture and mechanical properties. Mechanics of Materials 2011; 43 (9): 476-486.
[26] Wright J R, Sloan M R, Evans K E. Tensile properties of helical auxetic structures: a numerical study. Journal of Applied Physics 2010; 108 (044905).
[27] Mcafee J, Faisal N H. Parametric sensitivity analysis to maximise auxetic effect of polymeric fibre based helical yarn. Composite Structures 2017;162:1-12.
[28] Shen Y. Modelling of tensile properties of woven fabrics and auxetic braided structures by multi-scale finite element method [MSc thesis]. Auburn University; 2013.
[29] Sibal A, Rawal A. Design strategy for auxetic dual helix yarn systems. Materials Letters 2015;161:740-742.
[30] Miller W, Hook P B, Smith C W, Wang X, Evans K E. The manufacture and characterisation of a novel, low modulus, negative Poisson's ratio composite. Composites Science and Technology 2009; 69 (5) (2009) 651-655.
[31] Miller W, Ren Z, Smith C W, Evans K E. A negative Poisson's ratio carbon fibre composite using a negative Poisson's ratio yarn reinforcement. Composites Science and Technology 2012; 72 (7):761-766.
[32] Wright J R, Burns M K, James E, Sloan M R, Evans K E. On the design and characterisation of low-stiffness auxetic yarns and fabrics. Textile Research Journal 2012; 82 (7) (2012) 645-654.
[33] Zhang G, Ghita O, Evans KE. The fabrication and mechanical properties of a novel 3-component auxetic structure for composites. Composites Science and Technology 2015;117:257-267.
[34] Jiang N, Hu H. A study of tubular braided structure with negative Poisson’s ratio behavior. Textile Research Journal 2018; 88(24) 2810-2824.
[35] Jiang N, Hu H. Auxetic Yarn Made with Circular Braiding Technology. Physica Status Solidi (b) 2018; 1800168.
[36] Alpyildiz T. 3D geometrical modelling of tubular braids, Textile Research Journal. 2012;82(5) 443-453.
[37] Hu X, Wagoner RH, and Daehn GS. Comparison of explicit and implicit finite element methods in the quasistatic simulation of uniaxial tension. Communications in Numerical Methods in Engineering 1994;10(12): 993- 1003.
[38] Xiang XM, Lu G, Wang ZH. Quasi-static bending behavior of sandwich beams with thin-walled tubes as core. International Journal of Mechanical Sciences 2015; 103:55-62.
[39] Fathers RK, Gattas JM, You Z. Quasi-static crushing of eggbox, cube, and modified cube foldcore sandwich structures. International Journal of Mechanical

Sciences, 2015, 101-102:421-428.
[40] Nasim M S, Etemadi E. Three dimensional modeling of warp and woof periodic auxetic cellular structure. International Journal of Mechanical Sciences 136 (2018) 475-481.
[41] Zeng J, Cao H, Hu H. Finite element simulation of an auxetic plied yarn structure. Textile Research Journal 2018; DOI: 10.1177/0040517518813659.
[42] Fu MH, Chen Y, Hu LL. A novel auxetic honeycomb with enhanced in-plane stiffness and buckling strength. Composite Structures 2017;160:574-585.
[43] https://epsrc.ukri.org/newsevents/casestudies/blastproofcurtain/.